Inorganic Chemistry Communications 148 (2023) 110361

Contents lists available at ScienceDirect

Inorganic Chemistry Communications

journal homepage: www.elsevier.com/locate/inoche

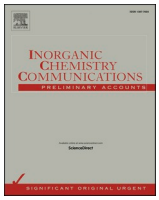

Short communication

Solar photocatalytic degradation of Methyl green on $CuFe_2O_4$/α Fe_2O_3 heterojunction

K. Rouibah [a,b], F.-Z. Akika [c], C. Rouibah [a], H.-R. Boudermine [a], S. Douafer [d], S. Boukerche [e], G. Boukerche [f], M. Benamira [c,*]

[a] Department of Process Engineering, University Mohamed Seddik Benyahia-Jijel, BP 98, Ouled Aissa, 18000 Jijel, Algeria
[b] Laboratory Materials: Elaboration-Properties-Applications LMEPA, University Mohamed Seddik Benyahia, BP 98, Ouled Aissa, 18000 Jijel, Algeria
[c] Laboratory of Materials Interaction and Environment (LIME), Department of Chemistry, University Mohamed Seddik Benyahia, BP 98, Ouled Aissa, 18000 Jijel, Algeria
[d] Department of Fundamental Studies of Science & Technology, University of Jijel, B.P. 98, Jijel 18000, Algeria
[e] Laboratory of Surfaces Engineering (L.I.S), University Badji Mokhtar Annaba, Algeria
[f] Department of Electrical Engineering, LEA Laboratory University Badji Mokhtar Annaba, Algeria

ARTICLE INFO

Keywords:
Adsorption
Photocatalysis
Methyl green
Co-precipitation
Sun light

ABSTRACT

The purpose of this work was to investigate the photocatalytic activity of $CuFe_2O_4$/α Fe_2O_3 heterojunction toward Methyl green (MG) under sun light irradiation. Structural and textural properties were characterized using X ray diffraction (XRD), Fourier Transform infrared (FTIR) spectroscopy, Scanning electronic microscopy (SEM) and Brunauer, Emmet and Teller (BET) methods. UV–vis diffuse reflectance was used to evaluate the optical band gap energy ($E_g = 1.83$ eV) which confirmed the semiconductor character of the prepared material. To construct the energy band diagram, conducting and valence bands positions were determined using the predicted flat band potential (V_{fb}) of $CuFe_2O_4$ (0.51 V/SCE) and α-Fe_2O_3 (- 0.18 V/SCE) from Mott-Schottky plots. The adsorption study of Methyl green was carried out using kinetic models and adsorption isotherms. The kinetic data were well fitted by pseudo-second order model and Langmuir isotherm was used as the best model to describe the adsorption of MG dye. The photocatalytic activity of the catalyst under solar light irradiation was followed by UV–vis spectroscopy. The photodegradation results showed the efficient of the $CuFe_2O_4$/α Fe_2O_3 heterojunction toward Methyl green with a yield of 91 % within 120 min.

1. Introduction

Numerous industrial sectors used dyes such as textiles, tanneries, stationary, food, plastics, pharmaceutics and cosmetics [1,2]. Their presence in the environment affects both the ecosystem quality and human health. Several studies have shown that these pollutants can be carcinogenic, mutagenic and teratogenic [2–5]. In aerobic conditions, dyes are hard to biodegrade due to their complex chemical structure and the presence of aromatic rings. As a result, the corresponding aqueous effluents necessitate special treatment because of the impact they have on natural environments. Conventional treatments like chemical oxidation, membrane processes, adsorption, coagulation and flocculation transfer pollution from an aqueous phase to a new phase and typically result in the formation of concentrated sludge, resulting in secondary waste problems or, more frequently, extremely costly materials regeneration [5–7].

Advanced oxidation processes (AOPs) including heterogeneous photocatalytic are widely used to degrade pollutants in aquatic environments through the generation of reactive oxygen species: superoxide ($\cdot O^{2-}$) and hydroxyl ($^{\cdot}OH$) radicals. AOPs have emerged in last years as effective methods for removing dyes in wastewater and appear to be the processes of choice because they make it possible to obtain a total degradation of the dyes at ambient pressure and temperature and without the formation of the secondary toxic products [2,3,4,8]. The excitation of a semiconductor with irradiation energy at least equal to the band gap energy (BE) is the basis of photocatalysis. Among variables semiconductors used for dyes photodegradation, metal oxides have received substantial attention, more particularly; research has focused on the use of iron materials due to their magnetic properties which make easy the separation of the catalysts after the dye degradation and

* Corresponding author.
E-mail addresses: benamira18@yahoo.fr, m_benamira@univ-jijel.dz (M. Benamira).

https://doi.org/10.1016/j.inoche.2022.110361
Received 1 October 2022; Received in revised form 29 November 2022; Accepted 27 December 2022
Available online 29 December 2022

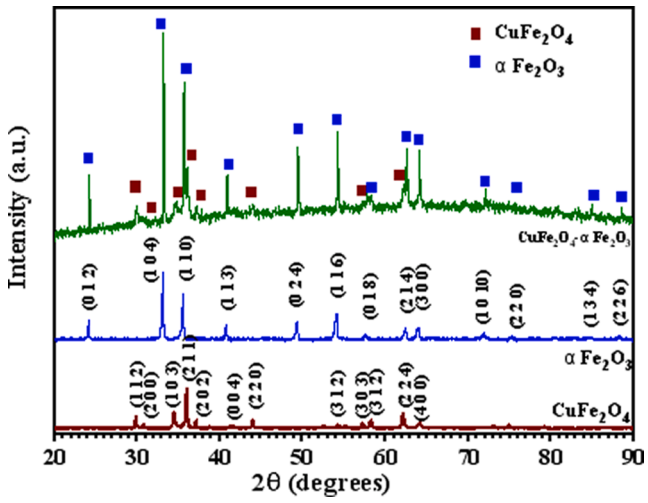

Fig. 1. The XRD patterns of the as prepared of $CuFe_2O_4$, α Fe_2O_3 and $CuFe_2O_4$/ α Fe_2O_3 (0.25:0.75).

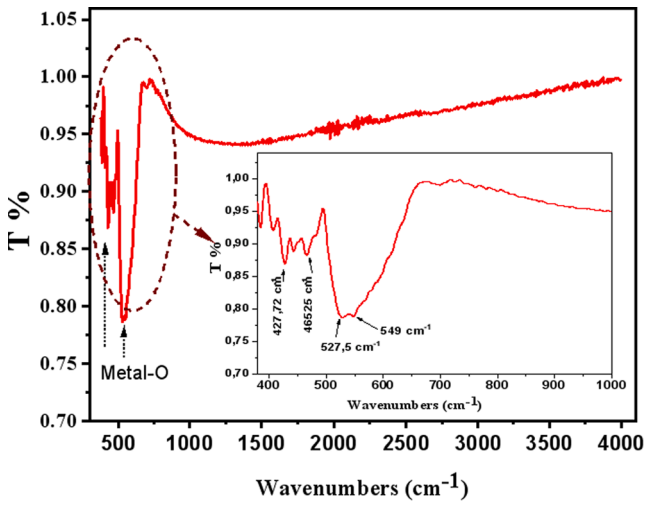

Fig. 2. FT-IR spectra of $CuFe_2O_4$/α Fe_2O_3 heterojunction.

because of the low band gap to absorb visible light [9–11].

Iron oxide α Fe_2O_3 (hematite) is n type semiconductor that exhibits good properties for photocatalytic degradation of pollutants: (1) low band gap (E_g = 2.1 eV) [12–15], (2) absorbs light up to 610 nm and captures up to 42 % of the energy from the solar spectrum [14,15], (3) stable and non-toxic (4) low cost and has a high resistance to photocorrosion [12,13].

However, the photocatalytic performance of α Fe_2O_3 can be limited by the recombination of the photogenerated electrons and holes (electronic lacuna h^+) [15]. Combining metal oxide to form heterojunction photocatalysts is an effective way to reduce the recombination rate of e^-/ h^+ providing more reaction actives sites [2,16–18]. In several works α Fe_2O_3 was coupled with other semiconductors to improve the photocatalytic activity for dyes degradation [16,18]. Li et al [19] have synthesized flower-like Ag_2O/Fe_2O_3 p-n heterojunctions by solvothermal precipitation–deposition method and shown that the heterojunctions exhibited under visible light irradiation a higher catalytic activity toward Rhodamine B than the pure αFe_2O_3. R. Guo et al [20] prepared Ag_2CO_3/αFe_2O_3 heterojunction using a facile ultrasonic precipitation strategy and then the catalyst was tested for the degradation of four dyes under sun light. It was found that the heterojunction significantly increased the photodegradation of Malachite green and Tartazine dyes. In another study, g-CN_4/ Fe_2O_3 heterojunction photocatalyst was prepared via the polycondensation method by Babar et al., and the photocatalytic performance was evaluated in the discoloration of Methyl orange and textile effluents (TE) under sun light. The results revealed that the catalyst displayed a better photocatalytic activity (99 % for MO, 97 % for TE) than Fe_2O_3 (8 % for MO,12 % for TE) and g-CN_4 (38 % for MO, 35 % for TE) [21]. Moreover, spinel ferrite has attracted much attention in the last years, they are considered excellent candidates for dye photodegradation and other organic pollutants [7,22]. In addition to their good optical and magnetic properties, the spinel structure of transition metals yields ions at their octahedral sites, which exchange with the tetrahedral sites to boost the photodegradation of pollutants [23].

Copper ferrite ($CuFe_2O_4$) is one of the ferrite spinels intensively studied owing to its low band gap of (1.4–1.5 eV) [24,25], superior catalytic activity [26], and high thermal and photocatalytic stability [24,25]. Doped, combined and pure $CuFe_2O_4$ catalysts were used for the dye degradation under UV and visible light illumination. For example, M.K. Attar Kar et al. [11] have studied the photodegradation of Direct red 264 under a visible lamp by $CuFe_2O_4$ and Zn-doped $CuFe_2O_4$ prepared by sol–gel auto-combustion method. They obtained a degradation efficiency of 94 % after 120 min of irradiation with CuF_2O_4 and a total discoloration with Zn-doped $CuFe_2O_4$ after only 60 min.

K. Atacane et al [27] have investigated the efficiency of $CuFe_2O_4$/ MoS_2 nanocomposite for Rhodamine B degradation under visible light. As a result, the $CuFe_2O_4/MoS_2$ p-n heterojunction was an excellent photocatalyst for dye removal with a dye removal efficiency of 98 **%.** In the study reported by T.P Oliveira et al [25], $CuFe_2O_4$ photocatalyst was tested for the photodegradation of Malachite green and Rhodamine B. The best rate of dye's discoloration was obtained with the catalyst treated at 400 °C. The authors have attributed this result on the one hand to the smaller size of the crystallites at 400 °C and in the other one to the presence of the hematite αFe_2O_3 as a secondary phase.

Herein a hetero-catalyst $CuFe_2O_4$/α Fe_2O_3 was prepared, characterized and tested for sun light photodegradation of cationic dyes taking Methyl green (MG) as the model molecule. Methyl green is a cationic dye that belongs to the class of triphenylmethane known for its high toxicity and is widely used in the textile industry. Nowadays, it's generally used in medicine and biology and as a photochromophore to sensitize gelatinous films [28–29]. The adsorption of MG dye onto $CuFe_2O_4$/α Fe_2O_3 surface is an essential step for effective degradation, therefore in the first step; the adsorption study was investigated.

2. Experimental

2.1. Catalyst preparation

Chemicals used are $Cu(NO_3)_2{\cdot}3H_2O$ (98 %, biochem Chemopharma), $Fe(NO_3)_2{\cdot}9H_2O$ (98 %, biochem Chemopharma) and NH_4OH (33 %, biochem Chemopharma). $CuFe_2O_4$ catalyst is synthesized by co-precipitation method using nitrates salts of Cu and Fe as precursors and ammonia as a precipitant agent. Nitrates salts of Cu and Fe used as precursors are dissolved separately in bidistilled water. The resultant solutions are then mixed, stirred magnetically and the NH_4OH solution is added until the pH reaches a basic value (pH ~ 10). The obtained precipitate is filtered, rinsed with ethanol and dried at 105 °C for 15 h. The obtained powder is ground and then calcined in air flow respectively at 300 °C to eliminate the nitrates, 500 °C and 900 °C during 4 h. Nitrates salts of Fe is used as precursors were dissolved separately in distilled water. Nitrates salts of Fe is used for the synthesis of α Fe_2O_3, 10 g is dissolved in 150 mL of distilled water under stirring at 80 °C for 20 min. 50 mL of NH_4OH solution is gradually added until reaching a pH of ~ 10. The resultant solution is heated at 90 °C under magnetic stirring for 4 h. The recuperated precipitate is treated at 650 °C/ 3 h and air quenched to avoid the conversion to Fe_3O_4.

The heterostructure $CuFe_2O_4$ /α Fe_2O_3 is prepared by a simple solid dispersion technique. 75 wt% of α Fe_2O_3 are added separately to 0.5 g of

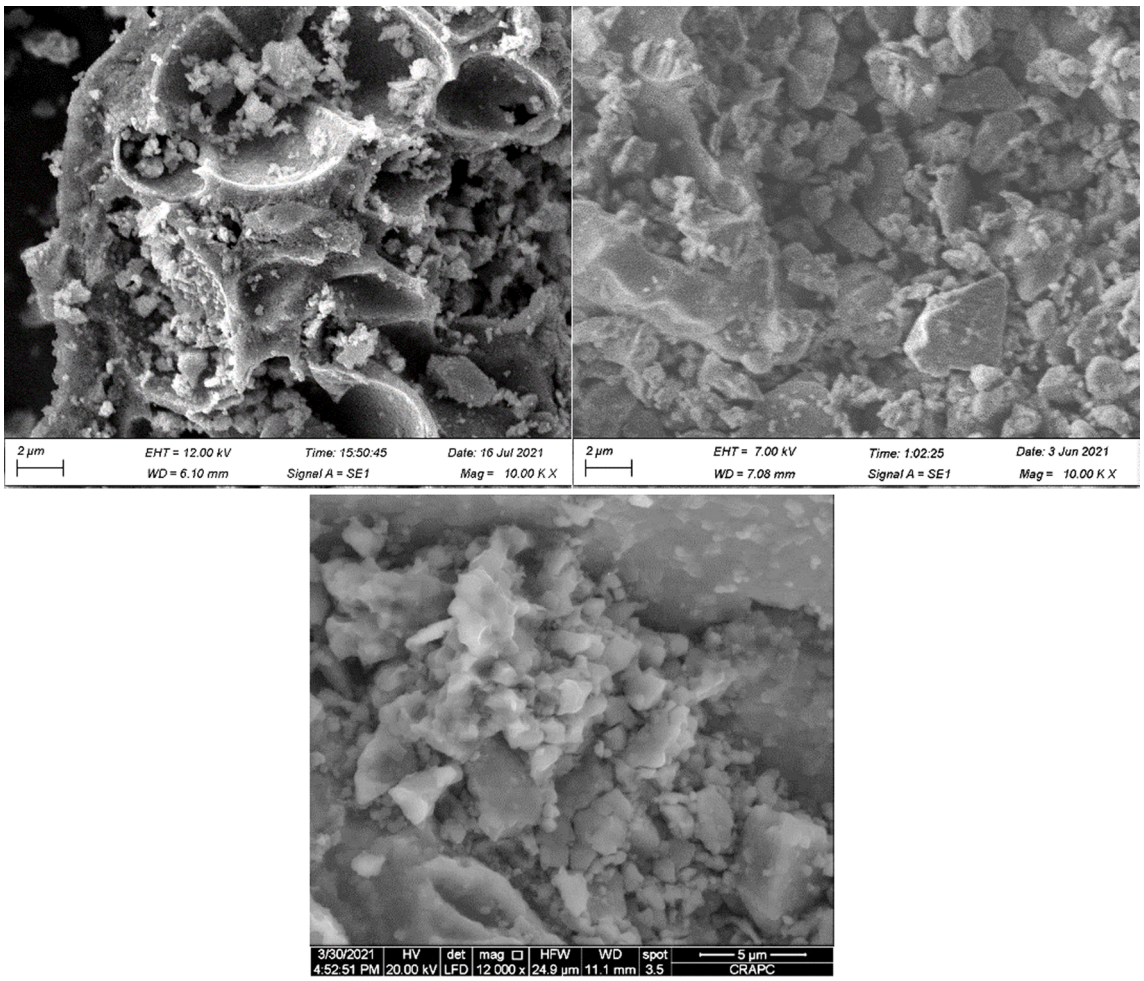

Fig. 3. SEM image of (a) $CuFe_2O_4$, (b) α Fe_2O_3 and (c) $CuFe_2O_4$/α Fe_2O_3 (0.25:0.75).

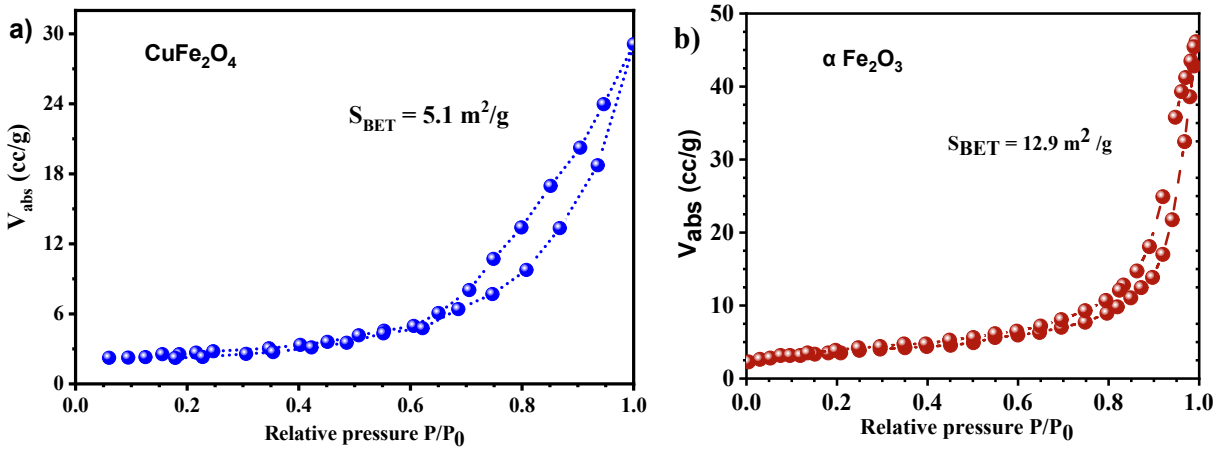

Fig. 4. N_2 adsorption/desorption isotherm obtained for (a) $CuFe_2O_4$, (b) α Fe_2O_3.

$CuFe_2O_4$. The as-prepared mixture is dissolved in methanol and placed in an ultrasonic bath and heated at 60 °C to remove the solvent. The obtained powder is dried in a hot air oven at 90 °C for 12 h.

2.2. Characterization techniques of the catalyst

XRD (X-ray powder diffraction) is carried out at room temperature utilizing Bruker D8 Advance diffractometer (Bruker) with Cu K_α radiation ($\lambda = 1.54$ Å). The patterns are collected with 0.018° step for a counting time of 5 s in the 2θ range of 20–90°. Fourier transform infrared (FTIR) analysis is done on a VERTEX70v (Bruker) spectrometer in the range of 400–4000 cm^{-1}. The sample's morphology is examined with a Zeiss EVO 15 scanning electron microscope. The specific surface area (S_{BET}) of the catalyst is determined by the Micromeritic 3Flex analyzer.

UV–vis spectrophotometer Specord 200 Plus is used to measure the

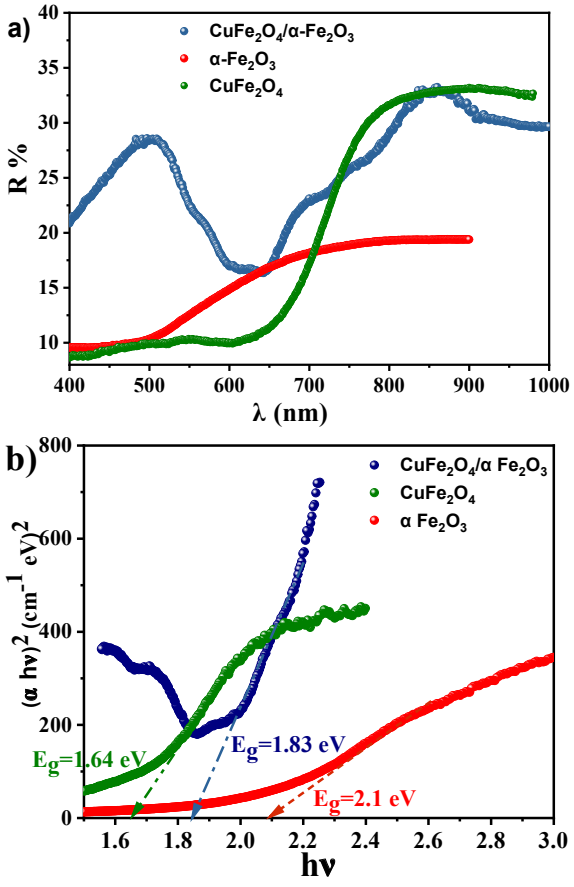

Fig. 5. (A) uv – vis diffuse reflectance spectra of $CuFe_2O_4$, α Fe_2O_3 and $CuFe_2O_4$/α Fe_2O_3, (b) Plots of the $(\alpha h\nu)^2$ vs photon energy (hν) for Direct optical transition.

diffuse reflectance spectrum, polytetrafluoroethylene (PTFE) is used as standard. The measurement is done on on the 400–1000 nm range.

Two-probe technique is used to measure the electrical conductivity on the 298 – 483 K temperature range. $CuFe_2O_4$ sample (1 cm^2) is prepared using uniaxial pressure and sintered at 900 °C for 1 h. The sample is introduced into resin epoxy and the side in contact with the solution is polished with silicon carbide papers (800, 1200).

A Solartron Analytical Potentiostat (1287A) is used for the photoelectrochemical (PEC) characterization. The PEC study is conducted in air at room temperature at a scanning rate of 5 mV s^{-1} using a standard cell. The silver lacquer assures the electrical contact between the working electrodes (Fe_2O_3, $CuFe_2O_4$) and Cu wires.

2.3. Adsorption and photodegradation of Methyl green

Adsorption experiments are carried out in batch system in the dark. A fixed mass of the catalyst is introduced into a determined volume of solution with a well-determined initial concentration. The solutions are kept in total darkness with constant stirring for the entire contact time chosen at a fixed temperature. The solid–liquid separation is carried out by filtration using a 0.45 μm millipore filter and then the solution is analysed to estimate the residual concentration of the MG dye using Shimadzu 1900 UV–vis spectrophotometer at $\lambda = 632$ nm.

The amount of the adsorbed dye (q) is calculated using Eq. (1):

$$q = \frac{C_0 - C_t}{m} . V \quad (1)$$

Where q is the adsorption capacity (mg/g); C_0 and C_e are, respectively, the concentrations of the initial and residual dye (mg/L); V is the volume of MG solution (L) and m is the mass of the used catalyst (g).

The photodegradation of MG is carried out in a Pyrex cell, during the month of June. An adequate quantity of catalyst is suspended in 250 mL of MG fresh solution (30 mg/L, natural pH) under magnetic agitation; the effect of adsorbent rate is investigated for 0.25 and 1.

The solution of MG dye is first placed in the dark for 60 min to create the adsorption–desorption equilibrium; then, the reactor is exposed immediately to sun light (≈100 mW/cm^2) with 47 % of humidity. The temperature was fixed at 25 °C.

The aliquots are drawn at regular time intervals and centrifuged for 15 min at 2000 tr/min to remove the residual photocatalyst. The MG concentration is determined by a UV – visible spectrophotometer and the MG dye degradation rate is calculated by applying Eq. (2):

$$\text{Degradation } \% = \left(1 - \frac{A_t}{A_0}\right) \text{x } 100 \quad (2)$$

Where A_0 and A_t are the absorbance of MG solution at initial time 0 and time (t), respectively.

3. Results and discussion

3.1. Structural, textural and optical properties

The XRD powder patterns of the as prepared materials $CuFe_2O_4$, α Fe_2O_3 and $CuFe_2O_4$ /α Fe_2O_3 are shown in Fig. 1. All peaks of the Fe_2O_3 pattern (Fig. 1) are indexed and correspond well to rhombohedral hematite Fe_2O_3 phase (α-Fe_2O_3) with space group *R-3c* (1 6 7) in agreement with the JCPDS Card N° 33–0664 [30,31]. The diffraction peaks of the copper ferrite correspond to the single spinel tetragonal structure $CuFe_2O_4$ (*I41/amd* (1 4 1), JCPDS 034–0425). The XRD pattern of the heterojunction reveal a presence of a mixture of hematite α Fe_2O_3 and copper ferrite $CuFe_2O_4$ indicating the successful formation of the heterosystem $CuFe_2O_4$/α Fe_2O_3. The main peaks are attributed to the hematite α Fe_2O_3 as the major phase (75 wt%) and the other peaks as attributed to the second phase of the heterostructure $CuFe_2O_4$.

Fig. 2 shows the FT-IR spectra of the hetero-structure $CuFe_2O_4$/α Fe_2O_3 obtained at 900 °C. We observed only the bands at high frequencies which characterize the metal oxygen bands; and no bands corresponding to water molecule or other organic compounds are shown in the FT-IR spectra. In copper ferrite $CuFe_2O_4$, metal ions are located in octahedral and tetrahedral sites close neighbors to oxygen ions [32]. Thus, the two absorption bands observed at about 527–549 cm^{-1} and 427–466 cm^{-1} correspond to the metal–oxygen bond of octahedral MO_6 and tetrahedral MO_4 sites, respectively [32,33]. The presence of two peaks in the same site predicts a probable inversion in the structure. for the band in the range 527–549 cm^{-1} is intense and so wide, that means it contains more than one type of bands Fe-O, in fact by comparison with the literature, the peaks absorption corresponding to the bending and stretching modes of the Fe-O band in hematite appear at about 533 and 440 cm^{-1} [34].

Surface morphology of the as-prepared materials is studied using SEM analysis as shown in Fig. 3. Fig. 3**a** shows the SEM image of the as-prepared $CuFe_2O_4$ particles prepared by co-precipitation method. Agglomerates composed of several connected particles are observed and a large porosity is observed. In the case of hematite, the nanoparticles are well-connected and agglomerated in small and large sizes. For $CuFe_2O_4$/α Fe_2O_3 heterojunction, the SEM image confirms the presence of agglomerates constituted by several particles of different sizes. Relatively homogeneous distribution is observed where it is hard to differentiate between the two constituents of this heterojunction.

The N_2 adsorption–desorption of $CuFe_2O_4$ and α Fe_2O_3 catalysts are shown in Fig. 4. $CuFe_2O_4$ exhibits IV type isotherm with H1 hysteresis loop attesting the presence of mesopores. Brunauer–Emmett–Teller (BET) method is used to determine the surface area based on the adsorption–desorption isotherms. For α Fe_2O_3 (Fig. 4 (b)), it exhibits a

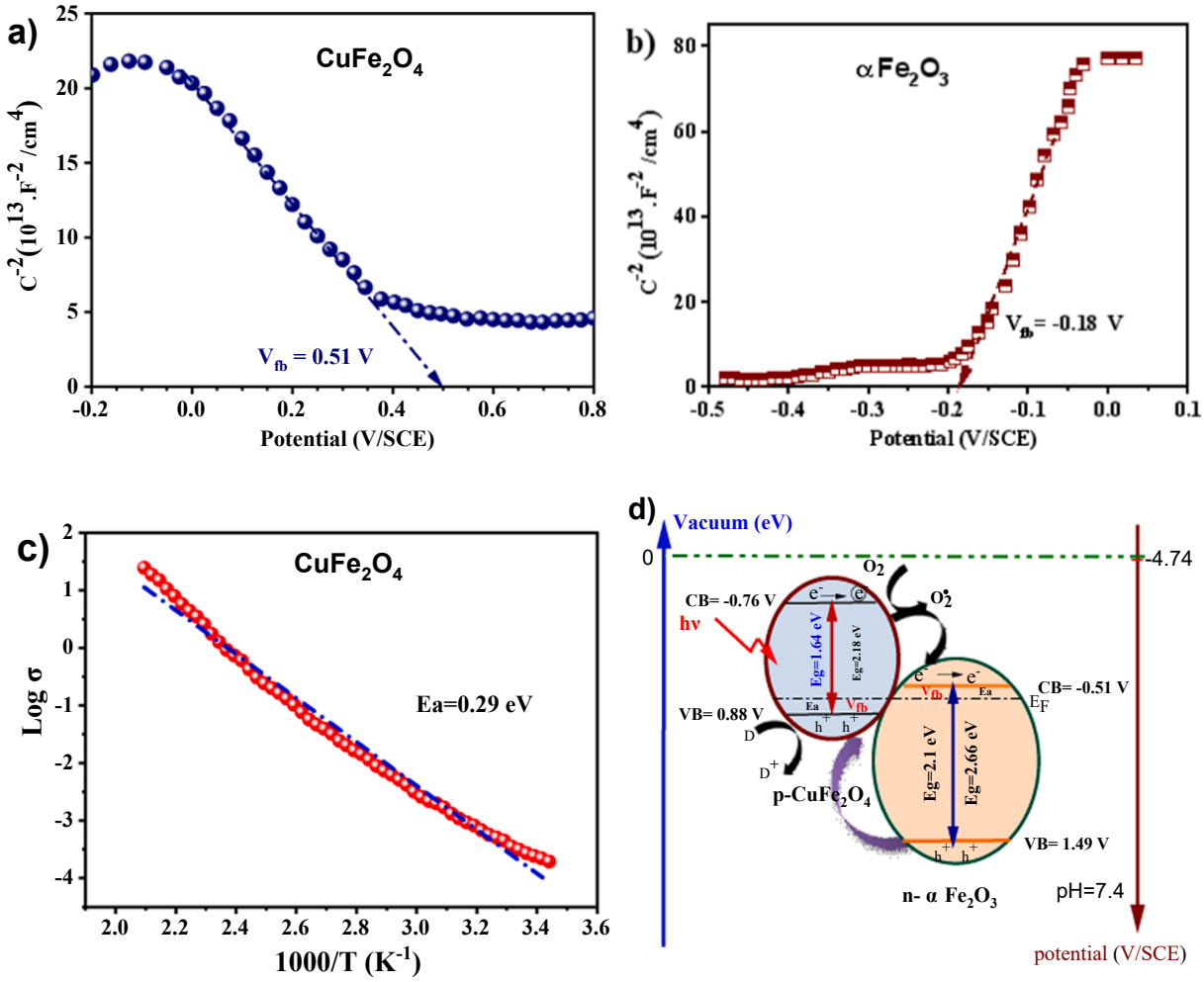

Fig. 6. The Mott Schottky plots of a) $CuFe_2O_4$, (b) α Fe_2O_3 (pH ~ 7.5, electrolyte. 0.5 M Na_2SO_4, frequency 10 kHz), (c) Thermal variation of the electrical conductivity, d) The energy band diagram of the hetero-system p-$CuFe_2O_4$/n-α Fe_2O_3/electrolyte.

Table 1
Crystallographic information and physico-chemical properties of $CuFe_2O_4$ and α Fe_2O_3.

Parameters	$CuFe_2O_4$	α Fe_2O_3
Space group	*I*41/*amd* (141)	*R*-3*c* (167)
$S_{BET}(m^2g^{-1})$	5.1	12.9
E_g (eV)	1.64	2.1
E_a (eV)	0.29	0.45
V_{fb} (V_{SCE})	0.51	− 0.18 V
pH_{pzc}	6.1	7.0
E_{VB}	0.88 V_{SCE} / −5.62 eV	1.49 V_{SCE}/ −6.23 eV
E_{CB}	−0.76 V_{SCE} / −3.98 eV	−0.51 V_{SCE}/ −4.13 eV

combination of type I and IV isotherms; at relative pressure less than 0.4, the adsorption isotherm shows a high adsorption, attesting that the Fe_2O_3 powder holds micropores (type I). On the other hand, in the relative pressure region between 0.45 and 1.0, the curve presents a hysteresis loop confirming the existence of mesopores (type IV). According to the BET analysis, specific surface area (S_{BET}) of the α Fe_2O_3 particles is relatively higher (12.9 m^2/g) than that of $CuFe_2O_4$ (5.1 m^2/g).

As known, the optical properties are very important in any photocatalysis study; so the obtained diffuse reflectance data of the as prepared materials are converted using the Kubelka–Munk function to estimate the optical gap energy (E_g) [35,36].

Therefore, E_g is determined from the intersection of a section of straight line with the x-axis, and the transition is directly permitted (Fig. 5b), with a value of 1.83 eV, which means that the heterojunction $CuFe_2O_4$/α-Fe_2O_3 may have visible-light photoactivity, which is beneficial for the use of visible-light and generating more charge carriers. The optical gap of α Fe_2O_3 and $CuFe_2O_4$ spinel are respectively 2.1 and 1.64 eV.

3.2. Electrochemical and electrical study

To determine the band positions of conducting and valence bands in order to construct the energy band diagram of p-$CuFe_2O_4$/n-α Fe_2O_3 hetero-system, the flat band potential (V_{fb}) is estimated by measurement of C^{-2} capacitance as a function of the electrode potential (V) using the Mott-Schottky equation (Eq. (3)) [37,38]:

$$C^{-2} = (2/eee_oN_A)[(V - V_{fb}) - kT/e] \quad (3)$$

Where C is the capacitance (F/m^2), e is the electron charge, ε is the relative permittivity, ε_o the permittivity of free space, N_D is the acceptor density (site/m^{-3}), k the Boltzmann constant and T the absolute temperature (K).

The value of V_{fb} for $CuFe_2O_4$ and α Fe_2O_3 semiconductors are estimated by extrapolating the linear part to the X-axis (Fig. 6(a) and (b)). A positive slope is observed for α Fe_2O_3 (Fig. 6a) indicating the n-type semiconductor behavior of α Fe_2O_3 (conduction by electrons) whereas, for $CuFe_2O_4$ (Fig. 6b), a negative slope was found which corresponds to a typical p-type. The flat band potential values for $CuFe_2O_4$ and α Fe_2O_3

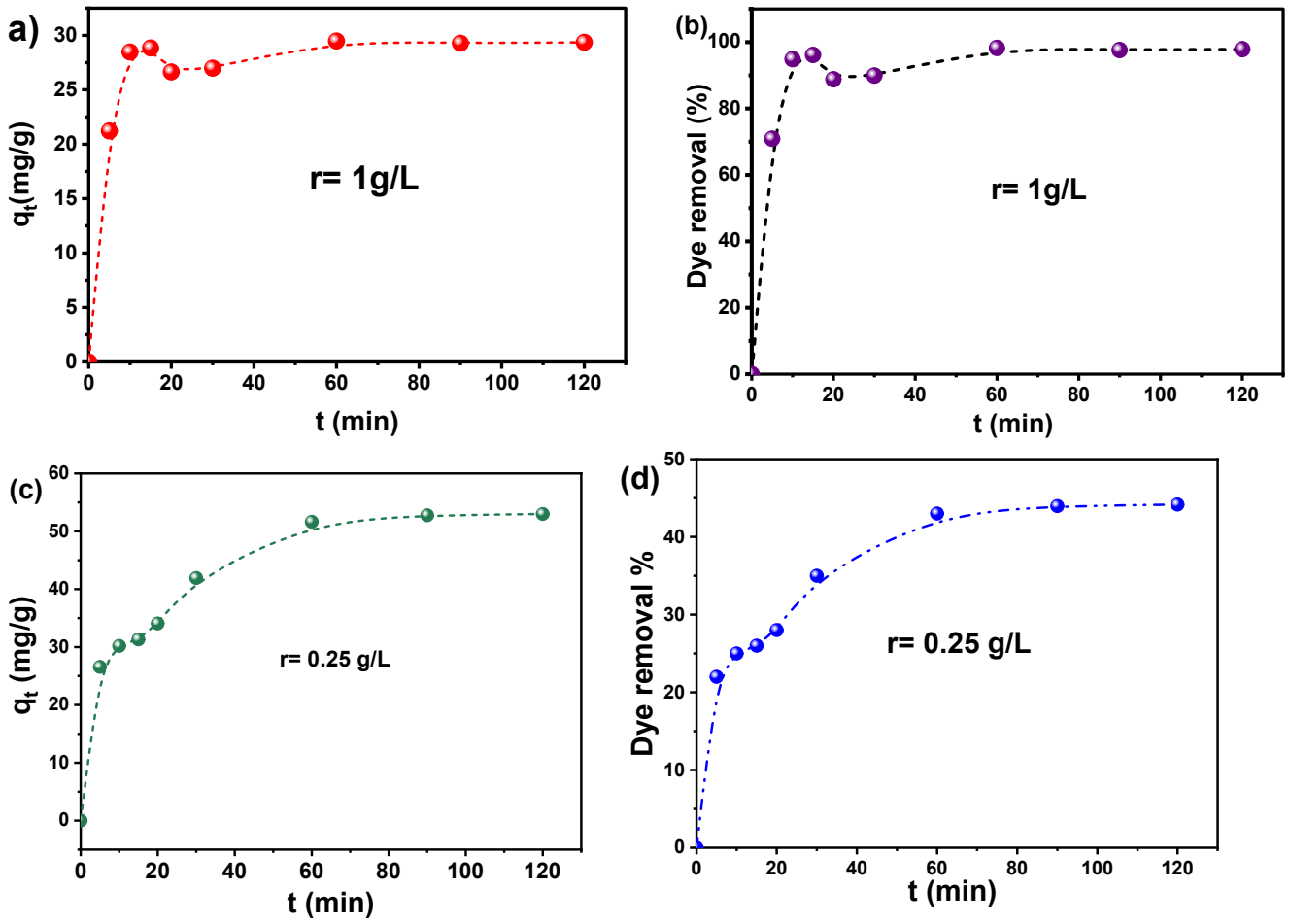

Fig. 7. Effect of contact time on MG dye adsorption onto $CuFe_2O_4$/α Fe_2O_3 catalyst for 1 and 0.25 g/L dose. Conditions. C_0 = 30 mg/L, pH = 7.4, T = 25C°.

Table 2
Kinetic parameters of MG adsorption for Catalyst dose (r) 0.25 and 1 g/L.

Catalyst dose (r) (g/L)	Pseudo 1st order $k_1(min^{-1})$	R^2	$q_{e,exp}$ (mg/g)	$q_{e,\ cal}$ (mg/g)	Pseudo 2nd order k_2 ($g.mg^{-1}.min^{-1}$)	R^2	$q_{e,exp}$ (mg/g)	$q_{e,\ cal}$ (mg/g)
1	5.47 10^{-2}	0.686	29.47	1.98	2.20 10^{-2}	0.999	29.47	29.77
0.25	0.02466	0.986	53	5.3	2.97 10^{-4}	0.995	53	58

are found as 0.51 and − 0.18 V/SCE, respectively. Their corresponding conducting band (CB) and valence band (VB) positions with respect to vacuum are calculated from the following formulas [39,40]:

$$EVB = eVfb + 0.059(pH - pHpzc) + Ea(typep) \quad (4)$$

$$EVB(vs.vacuum) = Ef - EVB(vs.NHE) \quad (5)$$

$$ECB = EVB - Eg \quad (6)$$

Where E_f is defined as the free electrons energy on the hydrogen scale (−4.5 eV), equivalent of − 4.74 eV between saturated calomel electrode potential and vacuum level potential at 25 °C.

The pHpzc value of $CuFe_2O_4$ and α Fe_2O_3 are evaluated by the pH drift method. pHpzc corresponds to the isoelectric points of $CuFe_2O_4$ and α Fe_2O_3 and has been determined to be 6.7 and 7.0, respectively, in total accord with the values published by Dang et al. [41] and Dehbi et al. [42]. According to the value of pHpzc of $CuFe_2O_4$ and α Fe_2O_3, the surface acquires a positive charge at pH < pHpzc, while it is negatively charged at pH > pHpzc.

The activation energie (E_a) is obtained from a logarithmic plot of the electrical conductivity vs a reciprocal temperature as shown in Fig. 6(c) for $CuFe_2O_4$ (E_a = 0.29 eV). E_a of Fe_2O_3 (0.45) is taken from the work of Cowan et al. [43].

The constructed energy band diagram of the hetero-system p-$CuFe_2O_4$/n-α Fe_2O_3/electrolyte presented in Fig. 6(d) is obtained according to the calculated positions of VB and CB of $CuFe_2O_4$ and α Fe_2O_3 (Table 1).

The potential/energy of p-$CuFe_2O_4$-CB (-0.76 V/-3.98 eV) is positioned more negative that the α Fe_2O_3 and the narrow band gap (1.64 eV) can easily generate the photoexcited (e^-/h^+) pairs. Due to the incorporation of *n*-type α Fe_2O_3, the photogenerated electron can be transferred to the α Fe_2O_3-CB (-0.51 V/-4.13 eV), whereas the hole (h^+) in the valence band (VB) of α Fe_2O_3 (1.49 V/-6.23 eV) can be transferred to p-$CuFe_2O_4$-VB (0.88 V/-5.62 eV). The band diagram confirms the construction of type-II heterojunction favorable for the charges separation and increases the lifetime of (e^-/h^+) pairs.

3.3. Adsorption and photocatalytic activity study

To examine the potential adsorption of the $CuFe_2O_4$ / α Fe_2O_3

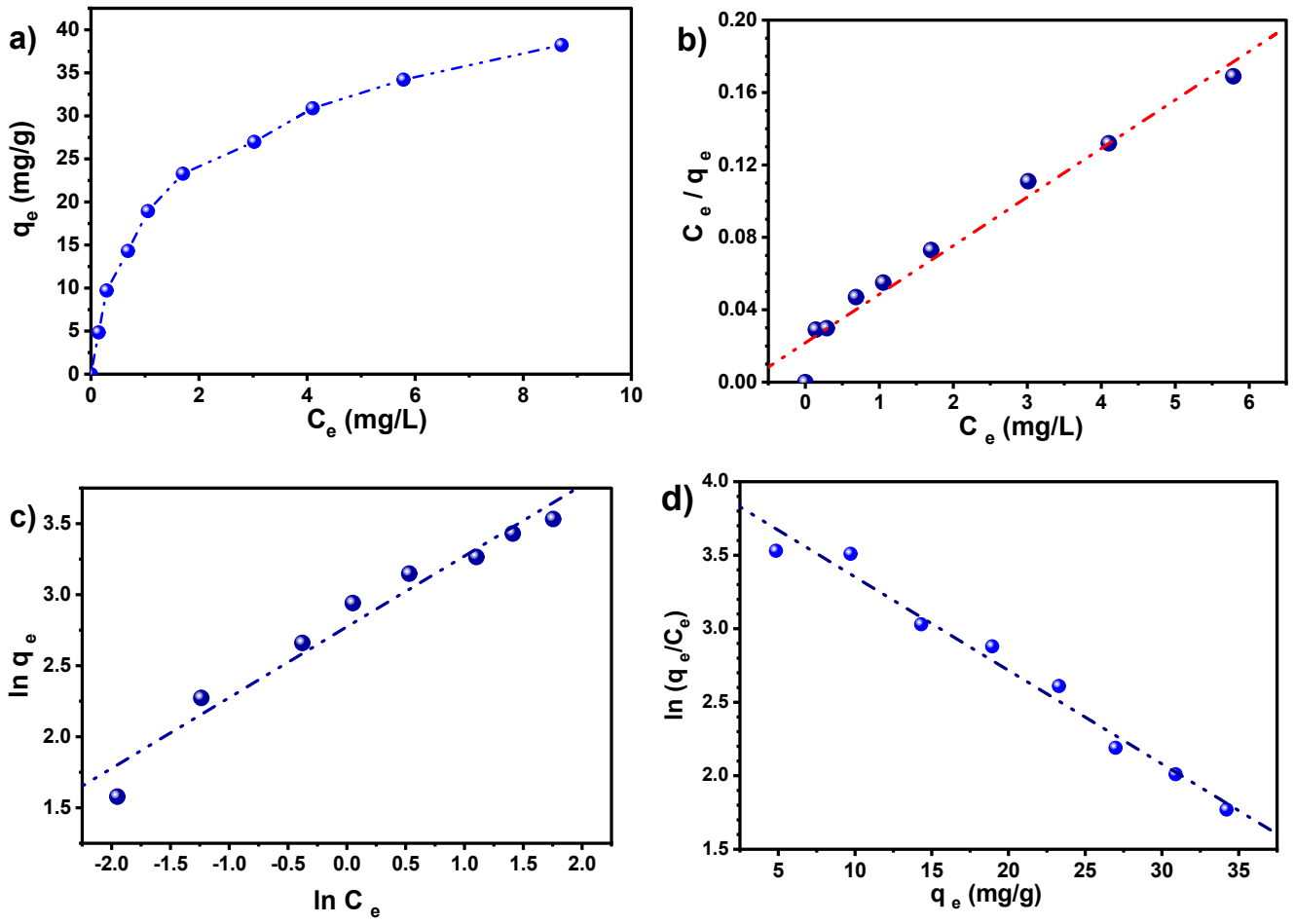

Fig. 8. (a) Adsorption isotherm of MG onto $CuFe_2O_4/\alpha\ Fe_2O_3$ catalyst, (b) Langmuir, (c) Freundlich and (d) Elovich model. Conditions. T = 25 °C; pH = 7.4, r = 1 g/L.

Table 3
Adsorption Parameters of Langmuir, Freundlich and Elovich isotherm models.

Model	Parameters		R^2
Langmuir II	q_m (mg/g)	K_L (ml/μg)	
	38.46	1.236	0.966
Freundlich	k_f(mg/g). (μg/ml)	1/n	
	16.013	0.498	0.960
Elovich	q_m (mg/g)	K_E (l/mg)	
	15.78	3.399	0.976

catalyst for MG dye, a kinetic study was investigated for a dye concentration of 30 mg/l at free pH and catalyst dose of 0.25 and 1 g/L. The adsorption kinetics depicts the evolution of the adsorption process versus time.

Fig. 7 presents the kinetics of MG adsorption. For 1 g/L dose Fig. 7 (a) and (b), a higher adsorption capacity of MG dye from the first five minutes (21.22 mg/g) is obtained with a removal efficiency of 70.7 %. At 60 min, equilibrium is reached and 98.23 % (29.47 mg/g) of the dye is adsorbed. This result can be explained by a great affinity of our catalyst towards MG. By decreasing the mass of the catalyst, the adsorption rate decreased up to 43.96 with an adsorption capacity of 52.76 mg/g, this result is simply attributed to the decrease of the surface area available, and hence the number of active sites. For 0.25 g/L dose Fig. 7 (c) and (d), the adsorption capacity of MG after just five minutes is 26.56. mg/g with a removal efficiency of 22 %. At 60 min, equilibrium is reached and 43 % (51.64 mg/g) of the dye is adsorbed.

The kinetic behavior of the adsorption process is fitted using the two surface reaction models: pseudo first order and pseudo second order (Eq. (7) and (8)).

$$\frac{dq_t}{dt} = k_1(q_e - q_t) \text{or } log(q_e - q_t) = logq_e - \frac{k_1}{2.303}t \quad (7)$$

$$\frac{dq_t}{dt} = k_2(q_e - q_t)^2 or \frac{t}{q_t} = \frac{t}{q_e} + \left[\frac{1}{k_2 q_e^2}\right] \quad (8)$$

Where q_e (mg/g) is the equilibrium adsorption capacity, q_t (mg/g) is the instantaneous adsorption capacity and k_1 and k_2 are the pseudo first and second kinetic rates, respectively.

According to the fitting results presented in Table 2, the adsorption of GM is well described by the pseudo-second-order model, the regression coefficient is close to the unity and the calculated equilibrium capacity ($q_{e,\ cal}$) is quite similar to the experimental one ($q_{e,exp}$). This model explicates surface adsorption, intra-particle diffusion and the external liquid film diffusion processes [44].

The study of the adsorption isotherm often provides some insights of adsorption mechanism, surface properties and affinity to adsorbent. The adsorption isotherm of Methyl Green on $CuFe_2O_4/\alpha\ Fe_2O_3$ catalyst is performed at 25 °C for concentrations ranging from 5 to 45 mg/L with a catalyst dose r = 1 g/L. According to Fig. 8 and Giles & al classification of adsorption isotherms [45], it is an L-type isotherm and the capacity of the maximum adsorption is 38.46 mg/g. Three isotherm equations are selected for modelling the adsorption isotherm data: Langmuir II, Freundlich, and Elovich. The corresponding fitting parameters are displayed in Table 3. Based on The regression correlation coefficient (R^2)

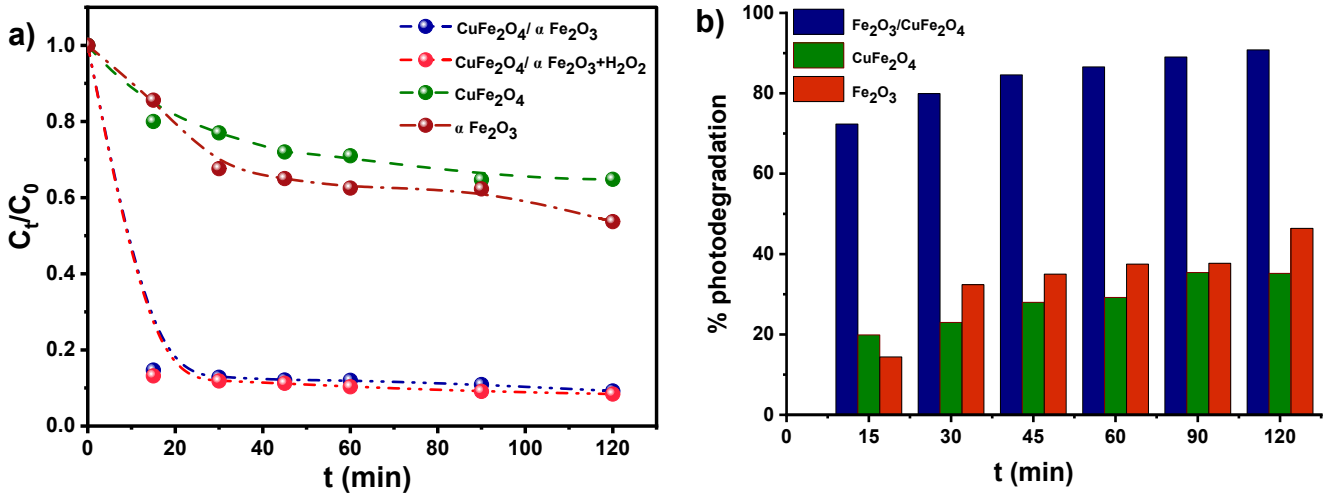

Fig. 9. Photodegradation kinetics of MG on $CuFe_2O_4$, α Fe_2O_3 and $CuFe_2O_4$/α Fe_2O_3 semi-conductors. Conditions. C_0 = 30 mg/L, pH = 7.4, T = 25 °C, r = 0.25 g/l.

Table 4
Kinetics parameters obtained from pseudo first model.

	k_{app} (min^{-1})	Standard deviation	R^2
$CuFe_2O_4$	0.0028	0.0002	0.97
α Fe_2O_3	0.0027	0.0003	0.95
$CuFe_2O_4$/α Fe_2O_3	0.0040	0.0004	0.96
$CuFe_2O_4$/α Fe_2O_3 + H_2O_2	0.0041	0.0003	0.98

Table 5
Comparison of the photocatalytic performance of $CuFe_2O_4$/α Fe_2O_3 with other materials.

Photocatalyst	Light source	Initial conditions	Degradation Efficiency	Ref
CdS nanoparticles	UV	C_0 = 10 ppm $r_{s/l}$ = 0.03 g/L	90 %	[46]
Ce dopted ZnO	UV	C_0 = 20 ppm $r_{s/l}$ = 2 g/L	100 %	[47]
$Ni_{0.10}La_{0.05}TiO_2$	Visible light	C_0 = 25 ppm $r_{s/l}$ = 0.8 g/L	90–98 %	[48]
ZnO-TiO_2/clay	UV	C_0 = 75 ppm $r_{s/l}$ = 1 g/L	98.7 %	[49]
$CuFe_2O_4$/α Fe_2O_3	Solar light	C_0 = 30 ppm $r_{s/l}$ = 0.25 g/L	91 %	This study

and the calculated maximum adsorption capacity (q_m), the equilibrium adsorption data are well described by Langmuir model. In fact, this result suggests that the adsorption of MG on the catalyst predominantly occurs in monolayers in the given of concentration range.

In this study, the photocatalytic activity of the $CuFe_2O_4$/α Fe_2O_3 catalyst is evaluated toward degradation of MG dye under solar light irradiation and the corresponding results are shown in Fig. 9. As shown, the discoloration process is very fast from the first minutes of exposure to solar light irradiation with discoloration efficiency of 91 % within 120 min.

In contrast, the decolorization is widely decreased in the presence of pure $CuFe_2O_4$ and α Fe_2O_3, and the dye removal of MG not exceed 35 and 46 % after 120 min, respectively (Fig. 9). This is due to the high recombination of the generated (e^-/h^+) pairs. The experimental results confirm that the $CuFe_2O_4$/α Fe_2O_3 heterojunction can generate more reactive species than those of the $CuFe_2O_4$ and α Fe_2O_3 under the sun light irradiation, which is mainly favorable to MG dye photodegradation.

Indeed, under solar light irradiation, the photoexcited electrons can transfer from p-$CuFe_2O_4$-CB (-0.76 V/-3.98 eV) to n-α Fe_2O_3-CB (-0.51 V/-4.13 eV) and holes from α Fe_2O_3-VB (1.49 V/-6.23 eV) to $CuFe_2O_4$-VB (0.88 V/-5.62 eV); the recombination of charge carriers is inhibited due to the effective separation and the formation of type II heterojunction, which significantly improves the % of dye removal and the photocatalytic activity in comparison with pure $CuFe_2O_4$ and α Fe_2O_3. Therefore, the highly reactive hydroxyl radicals ($^{\bullet}OH$) are generated by reaction of photo-excited e^- with H_2O on the surface of α Fe_2O_3 catalyst, which then attack the MG dye molecule because the α Fe_2O_3-VB (1.49 V) is more positive than the potential of the $OH^-/^{\bullet}OH$ (0.949 V vs SCE). The MG dye molecule may further decompose through several intermediate steps to the stable products. Moreover, the electrons on $CuFe_2O_4$-CB reduce O_2 to form superoxide $O_2^{\bullet-}$. The photodegradation of MG dye in the presence of H_2O_2 is slightly increased (92 %), which confirm the essential role of holes accumulated on $CuFe_2O_4$-VB to oxidize directly the MG molecules.

The kinetics of MG degradation is studied using the pseudo-first order model, and the apparent rate constant k_{app} (min^{-1}) is calculated by the relationship between ln(C_0/Ct) and the irradiation time mentioned below:

$$\mathrm{Ln}\left(\frac{C_0}{C_t}\right) = k_{app}t \quad (9)$$

Where C_0/C_t is the normalized MG concentration and t is the reaction time.

Kinetic parameters obtained from pseudo first model using linear regression are listed in Table 4. The coefficients (R^2) obtained from linear regression close to 1 confirms the validity of the model used, which fit well the experimental data. Furthermore, the order of K_{app} for pseudo first-order model is $CuFe_2O_4$/α Fe_2O_3 + H_2O_2 > $CuFe_2O_4$/α Fe_2O_3 > $CuFe_2O_4$ > α Fe_2O_3, so the high degradation rate is obtained by heterojunction than the pure $CuFe_2O_4$ and α Fe_2O_3.

The degradation efficiency of $CuFe_2O_4$/α Fe_2O_3 heterojunction for decomposing MG organic dye was compared with reported literature in Table 5. The degradation efficiency dependents on the experimental conditions including the light irradiation source, dosage of photocatalysts, and reaction time. As seen, the MG photodegradation obtained in this study is favorably compared with those obtained by others for C_0 = 30 mg/L.

4. Conclusion

The present study was dedicated on the removal of MG dye by $CuFe_2O_4$/α Fe_2O_3 heterojunction under solar light irradiation. The heterojunction ($CuFe_2O_4$ /α Fe_2O_3) was prepared by a simple solid dispersion technique. The energy band diagram of p-$CuFe_2O_4$/n-α

Fe_2O_3/electrolyte was constructed according to the optical and electrochemical properties of the as prepared $CuFe_2O_4$ and α Fe_2O_3 materials. Adsorption isotherm study of MG was done for concentrations ranging from 5 to 45 mg/L; which presents an L-type isotherm with a maximum adsorption capacity of 38.22 (mg/g). The equilibrium adsorption process was well described by Langmuir II model. The heterojunction presented a superior photocatalytic activity due to the slow recombination of photoexcited electron-hole pairs, 91 % removal efficiency of MG dye within 120 min. The photodegradation process of MG dye obeys to the first-order kinetic model.

CRediT authorship contribution statement

K. Rouibah: Investigation, Methodology, Writing – original draft. **F.-Z. Akika:** Formal analysis, Investigation. **C. Rouibah** Formal analysis, Investigation. **H-R. Boudermine:** Formal analysis, Investigation. **S. Douafer:** Investigation. **S. Boukerche:** Investigation. **G. Boukerche:** Investigation. **M. Benamira:** Conceptualization, Supervision, Writing – review & editing.

Declaration of Competing Interest

The authors declare that they have no known competing financial interests or personal relationships that could have appeared to influence the work reported in this paper.

Data availability

Data will be made available on request.

Acknowledgment

We appreciate the financial support from The Directorate-General for Scientific Research and Technological Development (DGRSDT, PRFU N° B00L01UN180120220001) and Socio-economic Impact Project N °06/ Univ Jijel/DGRSDT. Authors are thankful to Mr. H. Boulahbel from CRAPC for SEM analysis.

Data Availability

"The datasets are available from the corresponding author on reasonable request."

References

[1] L. Zou, Q. Wang, X. Shen, Z. Wang, M. Jing, Z. Luo, Fabrication and dye removal performance of magnetic CuFe2O4 @CeO2 nanofibers, Appl. Surf. Sci. 332 (2015) 674–681, https://doi.org/10.1016/j.apsusc.2015.01.176.
[2] H. Anwer, A. Mahmood, J. Lee, K.H. Kim, J.W. Park, A.C.K. Yip, Photocatalysts for degradation of dyes in industrial effluents: Opportunities and challenges, Nano Res. 12 (2019) 955–972, https://doi.org/10.1007/s12274-019-2287-0.
[3] R. Gherbi, M. Benamira, Y. Bessekhouad, Enhanced photoelectrochemical and photocatalytic properties of Mg-doped ZnMn2O4, J. Alloys Compd. 851 (2021), https://doi.org/10.1016/j.jallcom.2020.156797.
[4] E. Ra, Advances in Photo-catalytic Materials for Environmental Applications, Res. Rev. J. Mater. Sci. 04 (2016) 26–50, https://doi.org/10.4172/2321-6212.1000145.
[5] P.V. Nidheesh, M. Zhou, M.A. Oturan, An overview on the removal of synthetic dyes from water by electrochemical advanced oxidation processes, Chemosphere. 197 (2018) 210–227, https://doi.org/10.1016/j.chemosphere.2017.12.195.
[6] H. Lahmar, M. Benamira, S. Douafer, F.Z. Akika, M. Hamdi, I. Avramova, M. Trari, Photocatalytic degradation of crystal violet dye on the novel CuCr2O4/SnO2 hetero-system under sunlight, Optik (Stuttg). 219 (2020), 165042, https://doi.org/10.1016/j.ijleo.2020.165042.
[7] N.K. Gupta, Y. Ghaffari, S. Kim, J. Bae, K.S. Kim, M. Saifuddin, Photocatalytic Degradation of Organic Pollutants over MFe2O4 (M = Co, Ni, Cu, Zn) Nanoparticles at Neutral pH, Sci. Rep. 10 (2020) 1–11, https://doi.org/10.1038/s41598-020-61930-2.
[8] B. Viswanathan, Photocatalytic Degradation of Dyes: An Overview, Curr. Catal. 7 (2017) 99–121, https://doi.org/10.2174/2211544707666171219161846.
[9] U.C. Nanotube, T. Nanoparticle, Niyaz Mohammad Mahmoodi, Water Air Soil Pollut. 224 (2013) 1–8.
[10] M. Tang, X. Li, C. Gao, X. Li, H. Qiu, Adsorption performance of CuFe2O4/rGO nanocomposites towards organic dye, Mater. Chem. Phys. 185 (2017) 114–121, https://doi.org/10.1016/j.matchemphys.2016.10.012.
[11] M. Kamel Attar Kar, R. Fazaeli, F. Manteghi, M. Ghahari, Structural, Optical, and Isothermic Studies of CuFe2O4 and Zn-Doped CuFe2O4 Nanoferrite as a Magnetic Catalyst for Photocatalytic Degradation of Direct Red 264 Under Visible Light Irradiation, Environ. Prog. Sustain. Energy. 38 (2019) 13109. https://doi.org/10.1002/ep.13109.
[12] Y. Liu, N. Sun, J. Hu, S. Li, G. Qin, Photocatalytic degradation properties of α-Fe2O3 nanoparticles for dibutyl phthalate in aqueous solution system, R. Soc. Open Sci. 5 (2018), 172196, https://doi.org/10.1098/rsos.172196.
[13] S. Kiamouche, L. Messaadia, H. Lahmar, G. Rekhila, M. Trari, M. Benamira, Enhanced photocatalytic degradation of Ponceau S Red dye on the novel hetero-system Fe2O3/WO3 under solar light irradiation, React. Kinet. Mech. Catal. 135 (2022) 3411–3426, https://doi.org/10.1007/s11144-022-02313-8.
[14] X. Liu, K. Chen, J.J. Shim, J. Huang, Facile synthesis of porous Fe2O3 nanorods and their photocatalytic properties, J. Saudi Chem. Soc. 19 (2015) 479–484, https://doi.org/10.1016/j.jscs.2015.06.009.
[15] M. Mishra, D.M. Chun, α-Fe2O3 as a photocatalytic material: A review, Appl. Catal. A Gen. 498 (2015) 126–141, https://doi.org/10.1016/j.apcata.2015.03.023.
[16] F. Mukhtar, T. Munawar, M.S. Nadeem, M. Hasan, F. Hussain, M.A. Nawaz, F. Iqbal, Multi metal oxide NiO-Fe_2O_3-CdO nanocomposite-synthesis, photocatalytic and antibacterial properties, Appl. Phys A (2020) 126–588, https://doi.org/10.1007/s00339-020-03776-z.
[17] F. Mukhtar, T. Munawar, M.S. Nadeem, M.N. ur Rehman, S. Batool, M. Hasan, M. Riaz, K.ur Rehman, F. Iqbal, Highly efficient tri-phase TiO_2–Y_2O_3–V_2O_5 nanocomposite: structural, optical, photocatalyst, and antibacterial studies, J. Nanostruct. Chem. 12 (2022) 547-564. https://doi.org/10.1007/s40097-021-00430-9.
[18] Y. Lei, J. Huo, H. Liao, Microstructure and photocatalytic properties of polyimide /heterostuctured NiO–Fe_2O_3–ZnO nanocomposite films via an ion-exchange technique, RSC. Adv 7 (2017) 40621–40631, https://doi.org/10.1039/c7ra07611h.
[19] S. Li, S. Hu, K. Xu, W. Jiang, J. Hu, J. Liu, Excellent visible-light photocatalytic activity of p-type Ag_2O coated n-type Fe_2O_3 microspheres, Mater. Lett 188 (2017) 368–371, https://doi.org/10.1016/j.matlet.2016.11.106.
[20] R. Guo, X. Qi, X. Zhang, H. Zhang, X. Cheng, Synthesis of Ag2CO3/α-Fe2O3 heterojunction and it high visible light driven photocatalytic activity for elimination of organic pollutants, Sep. Purif. Technol 211 (2019) 504–513, https://doi.org/10.1016/j.seppur.2018.10.011.
[21] S. Babar, N. Gavade, H. Shinde, A. Gore, P. Mahajan, K.H. Lee, V. Bhuse, K. Garadkar, An innovative transformation of waste toner powder into magnetic g-C_3N_4-Fe_2O_3 photocatalyst: Sustainable e-waste management, J. Environ. Chem. Eng 7 (2019), 103041, https://doi.org/10.1016/j.jece.2019.103041.
[22] R. Tomar, A.A. Abdala, R.G. Chaudhary, N.B. Singh, Photocatalytic degradation of dyes by nanomaterials, Mater. Today Proc. 29 (2020) 967–973, https://doi.org/10.1016/j.matpr.2020.04.144.
[23] T. Tatarchuk, B. Al-Najar, M. Bououdina, M.A.A. Ahmed, Catalytic and photocatalytic properties of oxide spinels, Handb. Ecomater. 3 (2019) 1701–1750.
[24] Y. Yao, F. Lu, Y. Zhu, F. Wei, X. Liu, C. Lian, S. Wang, Magnetic core–shell CuFe2O4@ C3N4 hybrids for visible light photocatalysis of Orange II, J. Hazard. Mater. 297 (2015) 224–233.
[25] T.P. Oliveira, S.F. Rodrigues, G.N. Marques, R.C.V. Costa, C.G.G. Lopes, C. Aranas, A. Rojas, J.H.G. Rangel, M.M. Oliveira, Synthesis, Characterization, and Photocatalytic Investigation of CuFe2O4 for the Degradation of Dyes under Visible Light, Catalysts. 12 (2022) 623, https://doi.org/10.3390/catal12060623.
[26] Z. Zhu, X. Li, Q. Zhao, Y. Li, C. Sun, Y. Cao, Photocatalytic performances and activities of Ag-doped $CuFe_2O_4$ nanoparticles, Mater. Res. Bull 48 (2013) 2927–2932, https://doi.org/10.1016/j.materresbull.2013.04.042.
[27] K. Atacan, N. Güy, M. Özacar, Design and synthesis of magnetically separable $CuFe_2O_4$/MoS_2 p-n heterojunction for photocatalytic efficiency of Rhodamine B degradation, Colloid. Interface Sc. Commun 40 (2021), 100359, https://doi.org/10.1016/j.colcom.2020.100359.
[28] A. Nezamzadeh-Ejhieh, E. Shahriari, Photocatalytic decolorization of methyl green using Fe(II)-o-phenanthroline as supported onto zeolite Y, Journal of Industrial and Engineering Chemistry 20 (2014) 2719–2726, https://doi.org/10.1016/j.jiec.2013.10.060.
[29] C. Changchen, C. Shinlu, Mechanistic Studies of the Photocatalytic Degradation of Methyl Green: An Investigation of Products of the Decomposition Processes, Environ. Sci. Technol 41 (2007) 4389–4396, https://doi.org/10.1021/es062465g.
[30] M. Fedailaine, M. Trari, Photoreduction of Ni2+ under solar and artificial reactors on the hetero-junction (CuFe2O4/ZnO): Comparison between experimental and theoretical results, Mater. Today Commun. 31 (2022), 103665, https://doi.org/10.1016/j.mtcomm.2022.103665.
[31] N. Doufar, M. Benamira, H. Lahmar, M. Trari, I. Avramova, M.T. Caldes, Structural and photochemical properties of Fe-doped ZrO_2 and their application as photocatalysts with TiO_2 for chromate reduction, J. Photochem. Photobiol. A Chem. 386 (2020), 112105, https://doi.org/10.1016/j.jphotochem.2019.112105.
[32] R.D. Waldron, Infrared spectra of ferrites, Phys. Rev. 99 (1955) 1727–1735, https://doi.org/10.1103/PhysRev.99.1727.
[33] A. Pradeep, G. Chandrasekaran, FTIR study of Ni, Cu and Zn substituted nano-particles of MgFe $_2O_4$, Mater. Lett. 60 (2006) 371–374, https://doi.org/10.1016/j.matlet.2005.08.053.
[34] D. Trpkov, M. Panjan, L. Kopanja, M. Tadić, Hydrothermal synthesis, morphology, magnetic properties and self-assembly of hierarchical α-Fe_2O_3 (hematite)

mushroom-, cube-and sphere-like superstructures, Appl. Surf. Sci. 457 (2018) 427–438.
[35] L. Yang, B. Kruse, Revised Kubelka–Munk theory. I. Theory and application, JOSA A. 21 (2004) 1933–1941.
[36] M. Benamira, H. Lahmar, L. Messaadia, G. Rekhila, F.Z. Akika, M. Himrane, M. Trari, Hydrogen production on the new hetero-system Pr_2NiO_4/SnO_2 under visible light irradiation, Int. J. Hydrogen Energy. 45 (2020) 1719–1728, https://doi.org/10.1016/j.ijhydene.2019.11.064.
[37] K. Gelderman, L. Lee, S.W. Donne, Flat-band potential of a semiconductor: using the Mott-Schottky equation, J. Chem. Educ. 84 (2007) 685.
[38] H. Lahmar, M. Benamira, L. Messaadia, M. Hamdi, I. Avramova, M. Trari, Synthesis, physical and photo-electrochemical properties of Gd_2CuO_4, J. Alloys Compd. 816 (2020), 152629, https://doi.org/10.1016/j.jallcom.2019.152629.
[39] K. Telmani, H. Lahmar, M. Benamira, L. Messaadia, M. Trari, Synthesis, optical and photo-electrochemical properties of $NiBi_2O_4$ and its photocatalytic activity under solar light irradiation, Optik (Stuttg). 207 (2020), 163762, https://doi.org/10.1016/j.ijleo.2019.163762.
[40] R. Laouici, S. Douafer, H. Lahmar, G. Rekhila, M. Trari, M. Benamira, Elaboration and studies of physical and photo-electrochemical properties of La_2NiO_4 and its use with SnO_2 in photo-evolution of hydrogen under visible light irradiation, Optik (Stuttg). 236 (2021), https://doi.org/10.1016/j.ijleo.2021.166654.
[41] H.T. Dang, T.K. Le, Precursor chain length dependence of polymeric precursor method for the preparation of magnetic Fenton-like $CuFe_2O_4$-based catalysts, J. Sol-Gel Sci. Technol. 80 (2016) 160–167, https://doi.org/10.1007/s10971-016-4070-8.
[42] A. Dehbi, Y. Dehmani, H. Omari, A. Lammini, K. Elazhari, A. Abdallaoui, Hematite iron oxide nanoparticles (α-Fe_2O_3): Synthesis and modelling adsorption of malachite green, J. Environ. Chem. Eng. 8 (2020), 103394, https://doi.org/10.1016/j.jece.2019.103394.
[43] A.J. Cowan, C.J. Barnett, S.R. Pendlebury, M. Barroso, K. Sivula, M. Grätzel, et al., Activation energies for the rate-limiting step in water photooxidation by nanostructured α-Fe_2O_3 nd TiO_2, J Am Chem Soc 133 (26) (2011) 10134–10140, https://doi.org/10.1021/ja200800t.
[44] F.Z. Akika, M. Benamira, H. Lahmar, A. Tibera, R. Chabi, I. Avramova, M.T. Suzer, Structural and optical properties of Cu-substitution of $NiAl_2O_4$ and their photocatalytic activity towards Congo red under solar light irradiation, J. Photochem. Photobiol. A Chem. 364 (2018) 542–550, https://doi.org/10.1016/j.jphotochem.2018.06.049.
[45] C.H. Giles, D. Smith, A. Huitson, A general treatment and classification of the solute adsorption isotherm. I. Theoretical, J. Colloid Interface Sci. 47 (1974) 755–765, https://doi.org/10.1016/0021-9797(74)90252-5.
[46] S. Ali, F. Akbar Jan, R. Ullah, N. Ullah, UV-light-driven cadmium sulphide (CdS) nanocatalysts: synthesis, characterization, therapeutic and environmental applications; kinetics and thermodynamic study of photocatalytic degradation of Eosin B and Methyl Green dyes, Water Sci. Technol. 85 (2022) 1040–1052.
[47] K.S. Al-Namshah, S.M. Mariappan, M. Shkir, M.S. Hamdy, Photocatalytic degradation mechanism of Ce-loaded ZnO catalysts toward methyl green dye pollutant, Appl. Phys. A Mater. Sci. Process. 127 (2021) 1–10, https://doi.org/10.1007/s00339-021-04602-w.
[48] A. Kumar, G. Pandey, The photocatalytic degradation of Methyl Green in presence of Visible light with photoactive Ni0.10: La0 .05: TiO2 nanocomposites, J. App. Chem 10 (9) (2017) 31–44.
[49] H. Bel Hadjltaief, M. Ben Zina, M.E. Galvez, P. Da Costa, Photocatalytic degradation of methyl green dye in aqueous solution over natural clay-supported ZnO-TiO2 catalysts, J. Photochem. Photobiol. A Chem. 315 (2016) 25–33, https://doi.org/10.1016/j.jphotochem.2015.09.008.